**JOURNAL OF THEORETICAL AND APPLIED MECHANICS**
**60**, 3, pp. 479-494, Warsaw 2022
https://doi.org/10.15632/jtam-pl/151806

# PARAMETRIC ANALYSIS OF THE WHOLE LOADING PROCESS OF TRANSLATION-TORSION COUPLED VIBRATION CHARACTERISTICS OF THE MULTI-LAYER BI-DIRECTIONAL ECCENTRIC FRAME STRUCTURE[1]

Yuping Kuang

*School of Civil Engineering and Communication, North China University of Water Resources and Electric Power, Zhengzhou, China; e-mail: kuangyuping8826@163.com*

Yanshan Liu

*Renhe Design Engineering Group Co., Ltd., Zhengzhou, China*

Earthquake investigations confirm that irregular structures suffer more damage than their symmetric counterparts. The vibration mode of irregular structures is affected by the coupling of lateral and torsional vibration characteristics. The analysis of the lateral-torsional coupling effect is mainly limited to unidirectional eccentric structure or single-layer eccentric design. To fill this gap, this paper presents a parametric study of the whole loading process, exploring lateral-torsional coupling vibration characteristics of multi-layer bi-directional eccentric structures. The performed nonlinear static analysis revealed that the natural frequency of eccentric frames with different layers exhibited a general pattern with a three-stage evolution from elastic to elastic-plastic stages. Accordingly, three different elastic-plastic development stages of parametric analysis were defined. The effects of the uncoupled torsion-to--lateral frequency ratios $\Omega$ and stiffness eccentricities on the translation-torsion coupled vibration characteristics in the above three stages were simulated via self-compiled programs on the MATLAB platform. The results obtained show that the range of $\Omega$ controlling the vibration characteristics was related to the eccentricities. Therefore, it was proposed to set different limit values of $\Omega$ in designing and analyzing the structures with different bi-directional eccentric degrees. At $\Omega = 1.1 \sim 1.2$, the coupling effect between bi-directional eccentricities led to transformation between the first- and second-order vibration modes, while the direction with the lowest lateral stiffness could not be directly judged as the structure first-order principal vibration direction. In the third stage, when the bi-directional eccentricities reached or even exceeded 0.3, the second and third modes transformed into each other.

*Keywords:* eccentric structure, translation-torsion coupled, vibration characteristics, eccentricity, uncoupled torsion to lateral frequency ratio

## 1. Introduction

With the rapid development of modern architecture and more stringent customers' requirements for functionality of their buildings, an increasing number of buildings with non-traditional layouts has appeared. The enhancement of building functions and diversification of building forms determine the irregularity in structural configuration, leading to various eccentricities (Raheem *et al.*, 2018a,b; Sneha and Durgaprasad, 2022). Under the seismic action, the eccentric structures show translation-torsion coupled effects to some degree because of the non-coincidence between the floor mass center and rigidity center as well as the non-collinearity between the structure

[1]Paper presented at the 5th International Conference on Material Strength and Applied Mechanics, MSAM 2022, Qingdao, Shandong, China

inertia force and the induced resistance. Many seismic damage results demonstrate that apparent torsional failures easily occurred in the structures, especially eccentric ones, which accounts for a significant share of earthquake-induced damage (Kewalramani and Syed, 2020; Alaa *et al.*, 2022). Stathopoulos and Anagnostopoulos (2005) established a 3D model of three- and five-story bi-directional eccentric structures and conducted elastic-plastic time-history analysis under a bi--directional seismic action. According to their research, "flexible sides" in multi-layer eccentric structures exhibited more significant ductility requirements than the "rigid sides", significantly different from the analysis results based on the single-layer simplified models (Stathopoulos and Anagnostopoulos, 2003). Halabian and Birzhandi (2014) investigated seismic responses of multi-layer bi-directional eccentric frame-shear wall structures with mass, stiffness and mixed (mass/stiffness) eccentricities in the elastic-plastic stage under the bi-directional earthquake effect, respectively. They found that the additional ductility requirements to the "flexible sides" with stiffness eccentricity were lower than the requirements to other types of eccentricity. Comparative studies of Stathopoulos and Anagnostopoulos (2003; 2005) and Halabian and Birzhandi (2014) revealed that different models applied to various eccentricity types might yielded contradictive predictions, i.e., elastic-plastic stage characteristics of single-layer eccentric structures differed from those of multi-layer ones. Rashidi *et al.* (2017) carried out a comprehensive 3D study on the effects of stiffness and strength eccentricities on the torsional behavior of a building model under unidirectional earthquake impact conditions. Although they proved that the stiffness eccentricity played a minor role in the torsional behavior of ductile systems, that finding was based only on a single-layer unidirectional eccentric shear wall structure and could not be directly extended to the multi-layer bi-directional eccentric frame structure. Georgoussis and Mamou (2018) investigated the effect of mass eccentricities on the seismic torsional response of medium-height multi-story buildings, focusing on the overall seismic response of the buildings. They clarified how the torsional response of a structure was influenced by an arbitrary spatial combination of mass eccentricities. However, the above study was mainly related to mass-eccentric systems. In particular, the stiffness eccentricity induced by the biased center of mass and rigidity mainly controlled the torsional behavior of buildings excited by seismic forces (Sneha and Durgaprasad, 2022). However, the change of the translation-torsion coupled effect in the elastic-plastic stage of the multi-story eccentric structure with stiffness eccentricities caused by the irregular layout of the plane needs to be further explored. Raheem *et al.* (2018a,b) investigated structural seismic response demands for the class of L-shaped buildings by evaluating the plan configuration irregularity of re-entrant corners and lateral-torsion coupling effects on the measured seismic response demands. The results proved that building models with high irregularity were more vulnerable to damage than regular ones due to excessive stress concentration and lateral-torsional coupling. Besides, Raheem *et al.* (2018) pointed out that the seismic design demands largely depended on the computational tools, inherent assumptions, and approximations adopted in the modeling process, making the introduction and verification of a special multi-layer eccentric model expedient. Khanal and Chaulagain (2020) evaluated the effect of plan configuration irregularity of different L-shaped models. They reported that current code provisions failed to account for the irregularities present within the buildings and had to be refined. Sneha and Durgaprasad (2022) conducted a parametric study on six kinds of ordinary asymmetric structures with different numbers of layers and structural walls at various positions and six types of unusual L-shaped buildings, as well as analyzed variation rules of the torsion coefficient of plane irregular buildings. Defining the torsion coefficient as the maximum story drift ratio at one end of the structure to the average displacement drift at two ends, they further proposed a new definition of the coefficient of torsional irregularity based on floor rotation. In addition, six models of L-shaped buildings were formulated with a gradual reduction in the plan of the regular reference building model. However, the eccentricity values of the above models were relatively scarce, limiting the scope of predicted results. Furthermore, they only analyzed the

eccentricity effect on the translation-torsion coupled without considering the specific influence of the uncoupled torsion-to-lateral frequency ratios, thus omitting this important influencing factor.

The above literature survey outlined the following three deficiencies of available approaches.

Firstly, the parametric patterns of single-layer eccentric structures in the elastic-plastic stage are not suitable for multi-layer eccentric structures in the same stage, so a multi-layer eccentric model should be introduced for parametric analysis.

Secondly, the analysis results on multi-layer eccentric structures in the elastic-plastic stage using various analytical models, eccentric types, parameter calculation methods, or input seismic waves differed. This can be attributed to the fact that the previous studies insufficiently accounted for the interaction between the biaxial stiffness eccentricity and the uncoupled torsion--to-lateral frequency ratios in the elastic-plastic stage of multi-layer bi-directional stiffness eccentric structures. Therefore, a systematic reference analysis is needed.

Thirdly, the vibration modes of eccentric structures under study exhibited the coupling of lateral and torsional vibration characteristics rather than the superposition of purely lateral or torsional modes. In the elastic stage, the vibration characteristics depend on the mass and stiffness matrices of the structure, being irrelevant to the external force. After entering the elastic-plastic stage, the structural lateral and torsional stiffnesses change, leading to changes in eccentricities, torsional-to-lateral frequency and vibration characteristics. Accordingly, the translation-torsion coupled effect in the elastic stage is no longer suitable for describing vibration characteristics in the elastic-plastic stage (Duan *et al.*, 1993). Scholars currently focus on the time-history dynamic analysis of eccentric structures while ignoring the inner mechanism of vibration characteristics of multi-layer eccentric structures at different stages of elastic-plastic development. This gap should be filled by performing parametric analysis of the whole loading process to investigate the internal mechanism.

In order to mitigate the above three problems, this study envisaged the following three research steps. Firstly, a simplified bi-directional eccentric multi-story building model is proposed, which can replace the original model in the inelastic analysis, yielding quite accurate results. Secondly, the nonlinear static analysis of the whole process is performed, proving that natural frequencies of asymmetrical frame structures with different floors follow a general trend of three-stage evolution from elastic to elastic-plastic stages. Accordingly, three different stages of elastic-plastic development are defined. Finally, variation rules of translation-torsion coupled vibration characteristics with change in uncoupled torsion-to-lateral frequency ratio $\Omega$ and bi-directional eccentricities during the entire loading process from elastic to elastic-plastic stages are examined in depth. The present research results are considered instrumental in the seismic design of irregular structures and respective theoretical studies.

## 2. Analytical model

This study uses a typical three-story bi-directional uniform eccentric frame structure as a case study for analysis. As shown in Fig. 1, the eccentric structure studied consists of $5 \times 3$ spans, the span in the $x$-axis direction is 6.9 m, and the span in the $y$-axis direction is 6.3 m. The influences of infill walls are not considered. The floor height is 3.9 m. Six frame columns ($K_{z1}$ in Fig. 1) have a cross-sectional size of $b_x \times h_y = 0.50\,\text{m} \times 0.55\,\text{m}$, while the remaining 18 frame columns have a cross-sectional dimension of $0.40\,\text{m} \times 0.45\,\text{m}$. The section height and width of the beams in the $x$-axis direction are 0.6 m and 0.25 m, respectively. And the section height and width of the beams in the $y$-axis direction are 0.55 m and 0.25 m, respectively. The section sizes of the secondary beams are $0.2\,\text{m} \times 0.4\,\text{m}$. The floor thickness is 0.1 m. And the strength of concrete is $C30$. According to the code for the load design of building structures (GB 50009-2012, 2012), the

standard value of the dead load on the floor surface is taken as $2.0\,\mathrm{kN/m^2}$. The standard value of the live load on the floor is subdivided into two areas, in which $3.0\,\mathrm{kN/m^2}$ is taken between axis $4 \sim 6$ and axis $C \sim D$, and $2.0\,\mathrm{kN/m^2}$ is taken for other parts. The deadweight of the beam, slab and column are calculated automatically by PKPM design software. According to the code for seismic design of buildings (GB50011-2010, 2016), the seismic fortification intensity is 7 degrees 0.2 g. The design group is the second group, the site category is class III, and the seismic grade is class III. The longitudinal reinforcement is HRB400, and the stirrup is HRB335. The important factor is equal to 1.0. The bottom of the structural model is consolidated, and the beam-column joints are rigid.

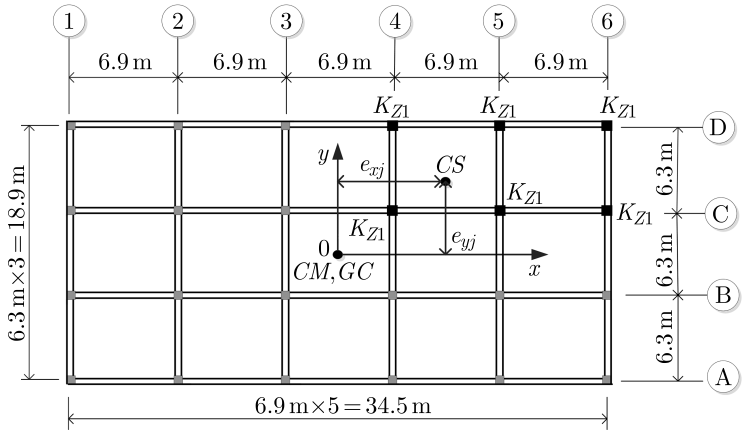


Fig. 1. A three-story bi-directional uniformly eccentric frame structure

In Fig. 1, $CM$ represents the mass center of each layer, and GC represents the geometric center of each layer. $CS$ (coordinates $(e_{xj}, e_{yj})$) represents the position of the stiffness center. It is called a single-layer eccentric structure when the floor stiffness center does not coincide with the mass center for a single-layer structure. As in multi-story buildings, the center of rigidity cannot be exactly defined; the static eccentricity of a multi-layer eccentric structure is calculated by an approximate method. It is extended from the concept of the eccentricity of a single-layer eccentric structure, which refers to the first moment center of the stiffness of lateral force resisting members of a certain layer. It can be calculated by the following formula

$$e_{xj} = \sum \frac{k_{yji} x_{ji}}{K_{yj}} \qquad e_{yj} = \sum \frac{k_{xji} y_{ji}}{K_{xj}} \tag{2.1}$$

in which $k_{xji}$ and $k_{yji}$ designate the stiffness of the $i$-th column of the floor $j$ in the $x$- and $y$-directions, respectively; $x_{ji}$ and $y_{ji}$ are the $x$ and $y$ coordinates of the $i$-th column of the floor $j$; $K_{xj} = \sum k_{xji}$, $K_{yj} = \sum k_{yji}$ represent the total translational stiffness of the floor $j$ in the $x$ and $y$ directions, respectively. The normalized stiffness eccentricities of the floor $j$ are defined as $b_{xj} = e_{xj}/r_j$, $b_{yj} = e_{yj}/r_j$, where $r_j$ is the radius of gyration of the mass center of the floor $j$.

When considering only the structures with stiffness eccentric induced by the asymmetrical plane arrangement of columns, it is stipulated that each member shows no change along the vertical direction. The engineering model under analysis is regarded as a multi-layer bi-directional regular eccentric structure, that is, a regular eccentric structure: the mass center and rigid center of the floor are on the same vertical axis, respectively; all floors have the same radius of gyration with respect to the center of mass. Previous studies have shown that (Yang *et al.*, 1988) this kind of eccentric structure has a stronger torsional response than other types of eccentric structures. Therefore, this paper takes the regular stiffness eccentric structures as the research object, and the stiffness eccentricity of each floor is the same. For the structural model shown in Fig. 1, the total lateral stiffness in the $x$-direction is $K_{xj} = 1.456 \cdot 10^7\,\mathrm{N/m}$, and the lateral

stiffness in the $y$-direction is $K_{yj} = 1.843 \cdot 10^7$ N/m. And the normalized stiffness eccentricities are $b_{x1} = b_{x2} = b_{x3} = b_x = 0.134$ and $b_{y1} = b_{y2} = b_{y3} = b_y = 0.208$, respectively.

To facilitate the parameter analysis of different $\Omega$ or eccentricities, a simplified eccentric model composed of two-way lateral-resisting members is introduced in this paper. The simplification model is a shear-torsional type series rigid plate layer model. The main assumptions are listed below.

(1) A horizontal steel sheet represents each floor system, and each degree of freedom (DoFs) of the floor is concentrated at the $CM$ of the floor. Three representative DoFs include two lateral DoFs along the $x$- and $y$-directions and one torsional DoF about the vertical axis.
(2) The mass center of each layer is located at the geometrical center. All mass centers are in the same line and have identical turning radii.
(3) The masses of various members and the floor are all concentrated at the $CM$ of the floor.
(4) The floor is absolutely rigid in its plane, and its out-of-plane stiffness is ignored. The out--of-plane stiffness of various lateral-resisting members and the torsional stiffness and axial deformations of the members are not considered.

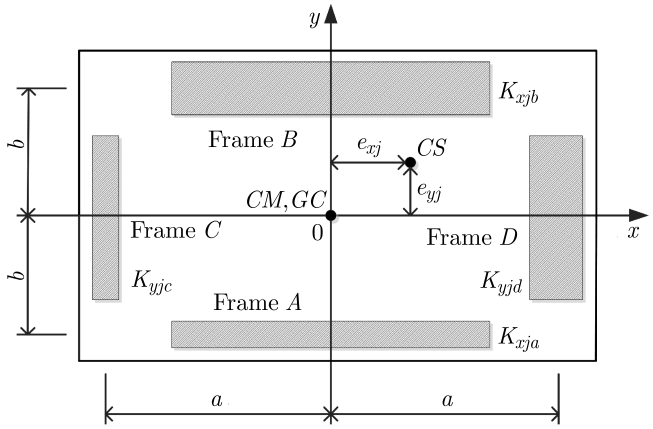


Fig. 2. A simplified model of the frame structure under study

Figure 2 illustrates the following simplifications of the frame structure under study. By merging the frame in the $j$-th layer along the $x$-axis direction in the original structure toward two sides, frame $A$ and frame $B$ can be formed, with a lateral stiffness of $K_{xja}$ and $K_{xjb}$, respectively, which are responsible for providing the lateral stiffness along the $x$-axis direction. By combining the frame in the $j$-th layer along the $y$-axis direction in the original structure towards two sides, frame $C$ and frame $D$ can be formed, with a lateral stiffness of $K_{yjc}$ and $K_{yjd}$, respectively, providing the lateral stiffness along the $y$-axis direction. Frames $A$ and $B$ are at a distance $b$ from the $x$-axis, while frames $C$ and $D$ are at a distance $a$ from the $y$-axis. According to the fact that the $j$-th layer of the simplified system and the $j$-th layer of the original system have equal total stiffness in the $x$ and $y$ directions, the torsional stiffness to the center of mass, and equal two-way eccentricities, the calculation formula of the simplified model can be deduced. More detail can be found elsewhere (Kuang *et al.*, 2018).

## 3. Analysis method

### 3.1. Nonlinear static analysis

The restoring-force model used in our paper is based on the member. The relation between the force acting on the lateral-resisting member and the displacement follows the bi-linear restoring

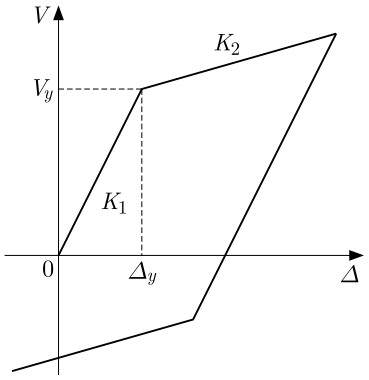


Fig. 3. The bi-linear restoring force model for each member

force model, as shown in Fig. 3. It is assumed that $K_1$ denotes the member stiffness in the elastic stage, $K_2$ represents the member stiffness after the yield and is approximately 10% of the stiffness before they yield, $\Delta_y$ denotes the column yield displacement, and $V_y$ represents the member yield shear. Their calculation formulae are written as (He and Ou, 2007)

$$V_y = \frac{2M_y}{H_n} \qquad \Delta_y = \frac{1}{(1-\eta)h_0}\frac{H^2 f_y}{6E_s} \tag{3.1}$$

in which $H$ and $H_n$ are the height and clear height of the column, respectively; $h_0$ represents the valid height of the column section; $f_y$ denotes the design value of the tensile strength of tensile steel; $E_s$ is the elastic modulus of the tensile steel; and $M_y$ and $\eta$ are the yield moment of the member section and the height coefficient of the concrete compressive region, respectively. $M_y$ and $\eta$ can be calculated by simplified formulas derived from the material stress-strain curves (Gao, 1988). The stress-strain of steel and concrete are illustrated in Fig. 4. $\sigma_y$ and $\varepsilon_y$ are the yield stress and yield strain of the steel, respectively; $f_c$ represents the design value of the axial compressive strength of concrete; $\varepsilon_0$ denotes the compressive strain of concrete when its compressive stress reaches $f_c$; $\varepsilon_{cu}$ is the ultimate compressive strain of concrete.

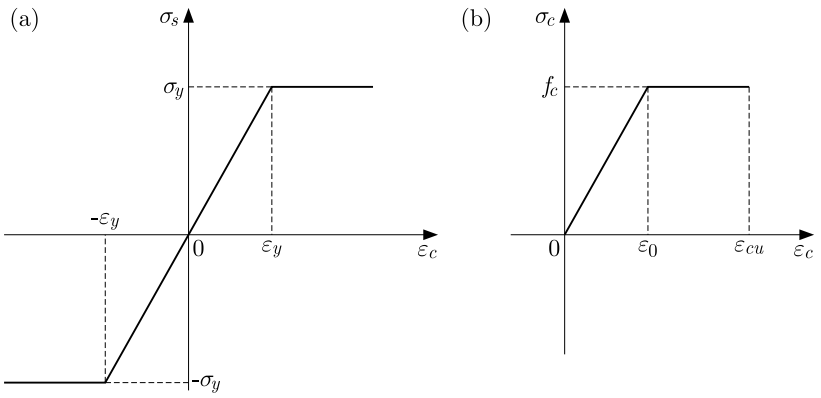


Fig. 4. The stress-strain relationship: (a) of steel, (b) of concrete

For the structural model analyzed in this paper, the yield displacement in the $x$- and $y$-directions of the members marked as $K_{z1}$ in Fig. 1 are $14.136 \cdot 10^{-3}$ m and $12.611 \cdot 10^{-3}$ m, respectively. Furthermore, the yield displacements in the $x$- and $y$-directions of the remaining members are $19.133 \cdot 10^{-3}$ m and $16.671 \cdot 10^{-3}$ m, respectively.

The M-language programming in MATLAB software implements nonlinear static analysis of the whole process. The inverted-triangle external static load is gradually applied to the structural mass center along the $x$-axis direction. The nonlinear problem is solved with the load increment

method. Under the $m$-level load increment, the total structural equilibrium equation can be written as

$$[\mathbf{K}_{m-1}\Delta\boldsymbol{\delta}_m = \Delta\mathbf{P}_m \qquad m = 1, \ldots, M \tag{3.2}$$

where $\mathbf{K}_{m-1}$ is the structural stiffness matrix recombined based on the member displacement and restoring force model after $(m-1)$ steps, $\Delta\boldsymbol{\delta}_m = [\Delta x_{1m}, \Delta x_{2m}, \Delta x_{3m}, \Delta y_{1m}, \Delta y_{2m}, \Delta y_{3m}, \Delta\theta_{1m}, \Delta\theta_{2m}, \Delta\theta_{3m}]$ is the incremental displacement vector of layer of each floor under the $m$-th load increment, and $\Delta\mathbf{P}_m = [\Delta P_{1m}, \Delta P_{2m}, \Delta P_{3m}, 0, 0, 0, 0, 0, 0]$ is the $m$-th load increment vector of the structure, and $\Delta P_{jm}$ can be calculated as

$$\Delta P_{jm} = \frac{w_j h_j}{\sum_{j=1}^{3} w_j h_j}\Delta V_{bm} \qquad j = 1, 2, 3 \tag{3.3}$$

where $\Delta P_{jm}$ designates the increment of the lateral load of the floor $j$ under the $m$-th load increment; $w_j$ is the representative value of gravity load of the floor $j$; $h_j$ is the height of the floor $j$; $\Delta V_{bm}$ refers to the increment of the base shear under the $m$-th load increment.

During the first loading step calculation, the structure initial stiffness matrix is set as the stiffness matrix $\mathbf{K}_0$. The initial stiffness matrix of the asymmetric plane structure can be established by the direct stiffness method (Chopra, 2006; Jiang and Kuang, 2016).

For the three-layer numerical example analyzed in this paper, the displacement of each layer of the floor after $m$-th steps can be written as

$$\boldsymbol{\delta}_m = [x_{1m}, x_{2m}, x_{3m}, y_{1m}, y_{2m}, y_{3m}, \theta_{1m}, \theta_{2m}, \theta_{3m}] = \boldsymbol{\delta}_0 + \sum_{n=1}^{m}\boldsymbol{\delta}_n \tag{3.4}$$

where $\boldsymbol{\delta}_0$ denotes the initial displacement vector of the structure.

The displacement of each member can be calculated according to the displacement of each layer and the coordinate of each column. The displacement of the $i$-th column in the $j$-th layer after the $m$-th step can be calculated as

$$u_{jim} = x_{jm} - \theta_{jm}y_{ji} \qquad v_{jim} = y_{jm} + \theta_{jm}x_{ji} \qquad j = 1, 2, 3 \tag{3.5}$$

where $x_{ji}$ and $y_{ji}$ represent the $x$- and $y$-direction coordinates of the $i$-th column in the $j$-th layer, respectively.

The case study is analyzed with software programming according to the above step. The member stiffness is adjusted based on the member restoring force model and the calculated displacement after each step. In this way, the non-synchronization of member displacement caused by floor torsion is considered in the entire analysis process. The loading stops until the interlaminar displacement angle of the layer reaches 1/50 of the value regulated in the Code for Seismic Design of Buildings (GB50011-2010, 2016).

### 3.2. Definitions of analysis stages

Figure 5 displays variation curves of the first three orders of the natural vibration frequency during the gradual loading process obtained using the original and corresponding simplified models with the loading coefficient $\alpha$. The latter is defined as the ratio of all applied loads after each load step to the total load on the system. The maximum value of $\alpha = 1$. As shown in Fig. 5, the first three orders of the natural vibration frequency obtained via the above two models are in good consistency during the whole loading process. They differ only slightly in the lateral force yield process, which further confirms reliability of the simplified model in replacing the original model for a series of parametric analyses in the elastic-plastic stage.

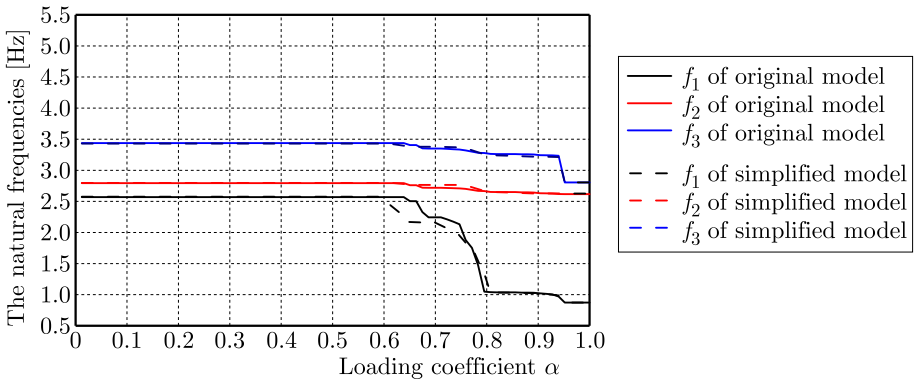


Fig. 5. The natural frequency versus the loading coefficient $\alpha$

Figure 5 illustrates that the natural frequency drops little by little from the elastic to elastic--plastic stage and shows prominent three-stage variation characteristics: a horizontal linear stage, a significant falling stage, approximately an oblique line, and a slight variation stage about a horizontal line. At $\alpha > 0.92$, the structure can be seriously fractured. This stage is ignored in the present parametric analysis. All members do not yield in the first stage, and the stiffness matrix does not change, so the frequency remains unchanged. In the second stage, the frequency varies the most, and this stage has the most significant impact on the vibration characteristics of the structure. According to the features of this change, the frequency in the second stage is simplified into an oblique straight line that changes linearly with $\alpha$ by using the least square method. This simplification is also convenient for parameter analysis. The frequency change in the third stage is similar to a horizontal straight line. To simplify the analysis, the average value is taken as the representative of this stage. To further validate the variation tendency of the natural vibration frequency of the multi-layer eccentric frame structure, the representative five and seven layers in the structure are also selected for further analysis. The model parameters and frequency variation curves of the five-layer eccentric frame structure and seven-layer eccentric frame structure can be found elsewhere (Kuang *et al.*, 2018). The frequency variation rules of the five and seven layers of the frame are similar to the three layers of the eccentric frame during the loading process, which can be subdivided into three stages. The frequency variations in the three stages can also be described by formulas

$$f_{1-1} = f_e \qquad f_{1-2} = k\alpha + s \qquad f_{1-3} = f_{e3} \tag{3.6}$$

where $f_e$ is the first-order natural frequency in the elastic stage of the structure; $k$ and $s$ are, respectively, the monomial coefficient and a constant term of the linear variation of the frequency in the second stage; and $f_{e3}$ is the third-stage frequency whose is equal to the average frequency of this stage.

As regards the three-layer eccentric frame structure in this study, the frequency variations [Hz] in the three stages can be described as follows

$$\begin{aligned} f_{31-1} &= 2.569 && \text{for} \quad \alpha \leqslant 0.664 \\ f_{31-2} &= -9.134\alpha + 8.633 && \text{for} \quad 0.664 < \alpha \leqslant 0.833 \\ f_{31-3} &= 1.028 && \text{for} \quad 0.833 < \alpha \leqslant 0.916 \end{aligned} \tag{3.7}$$

where $f_{31-1}$, $f_{31-2}$ and $f_{31-3}$ are the three-stage frequencies of the first-order frequency after simplified processing.

Figure 6 displays the variation rules of three-stage frequencies of the first-order frequency after simplified processing and the original frequency. Based on the variation characteristics of different stages, three stable stages of the parametric analysis are defined in this study. It can

also be seen from Fig. 6 that any point in the stage can represent the frequency values of the first and third stage. Since the second stage is an oblique straight line, the value in any point can be used as a representative one, while the values in other points can be obtained based on the linear relation. The point near the center should be selected to be more representative. In the whole analysis process, the displacements of the members perpendicular to the $x$-axis direction do not exceed the yield displacement, suggesting that the member is in the elastic stage. Therefore, only the condition of the lateral load-resisting members being in the elastic stage is analyzed in this study. Based on the interlaminar stiffness corresponding to each analyzed point in each layer at each stage and the other parameters of the eccentric structures at this stage, the stiffness matrix and the equation of motion at each stage could be determined by substituting the above parameters into the structure stiffness matrix to determine dynamic characteristics and perform the parametric analysis in different stages.

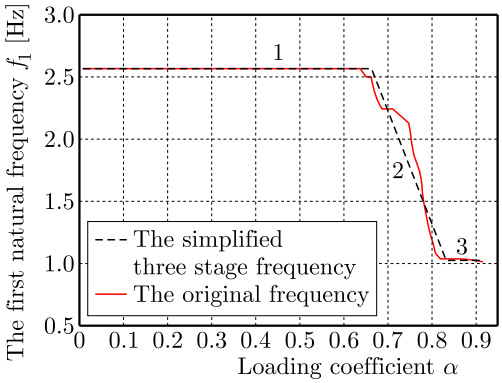


Fig. 6. The first natural frequency versus the loading coefficient $\alpha$

### 3.3. Calculation of mode direction factors

Each mode of an eccentric structure is the mode coupled with translation and torsion. The main vibration mode of the translation-torsion coupled vibration mode can be determined by mode direction factors (JGJ 3-2010, 2010). For the $i$-th vibration mode of the eccentric structure, $DX_i$ and $DY_i$ are defined as the mode direction factors of lateral mode shapes in the $x$-direction and $y$-direction, respectively. And $D\theta_i$ denotes the directional torsional factor. At $DX_i > 0.5$ or $DY_i > 0.5$, it is the lateral vibration mode, while at $D\theta_i > 0.5$, it is the torsional vibration mode. $DX_i$, $DY_i$ and $D\theta_i$ can be expressed as

$$DX_i = \sum_{j=1}^{n} m_j x_{ji}^2 \qquad DY_i = \sum_{j=1}^{n} m_j y_{ji}^2 \qquad D\theta_i = \sum_{j=1}^{n} m_j r_j^2 \theta_{ji}^2$$
$$DX_i + DY_i + D\theta_i = 1 \tag{3.8}$$

Table 1 shows the first three mode direction factors of asymmetrical multi-story buildings researched herein. The first vibration mode of the eccentric structure studied here is the lateral vibration mode along the $x$-axis direction, accompanied by lateral motion along the $y$-axis direction and torsion. The second mode is the lateral vibration mode along the $y$-axis direction, accompanied by lateral motion along the $x$-axis direction and torsion. The third mode is the torsional vibration mode, accompanied by lateral movement in two horizontal directions. In the below parametric analysis, $\Omega$ and the stiffness eccentricities are introduced as two main parameters. $\Omega$ is defined as the ratio of the first-order pure torsional frequency to the first-order pure lateral frequency along the $x$-direction of the equivalent symmetric system. The effects of $\Omega$ and the normalized stiffness eccentricities ($b_x$ and $b_y$) on the mode direction factors are evaluated.

**Table 1.** $DX_i$, $DY_i$ and $D\theta_i$ of the first three order modes

| Mode | 1 | 2 | 3 |
|---|---|---|---|
| $DX_i$ | 0.81 | 0.17 | 0.03 |
| $DY_i$ | 0.08 | 0.68 | 0.23 |
| $D\theta_i$ | 0.11 | 0.15 | 0.74 |

### 3.4. Verification of the simplified model

To further validate the accuracy and reliability of the proposed simplified model in the dynamic characteristic analysis, a corresponding 3D refined model for the three-story eccentric structure with its plane layout as in Fig. 1 is established. The beam element of BEAM188, which can define the cross-sectional dimension, is applied to simulate the frame beams and columns, and the shell element of SHELL63 is used to simulate the floor slab. The related structural parameters of the three-story eccentric structure are the same as those in Section 2. A detailed modeling process description can be found elsewhere (Kuang *et al.*, 2018). The first three vibration periods of the refined and simplified models are shown in Table 2, and the first three mode shapes of the refined model are shown in Fig. 7.

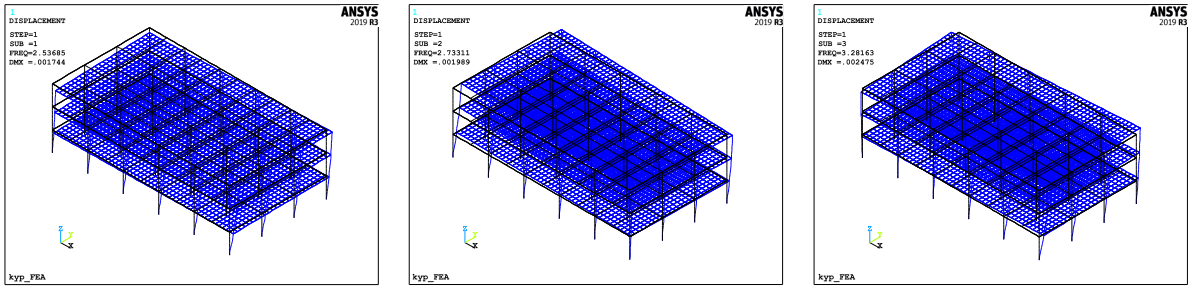


Fig. 7. The first three mode shapes of the refined mode: (a) first mode, (b) second mode, (c) third mode

Comparing the calculation results of the two models in Table 2, it can be seen that the relative error between the third-order natural frequency of the simplified model and the first three-order natural frequency of the refined model is within 5%, which verifies the rationality of the simplified model and also shows that the analysis using the simplified model is accurate and reliable. It can be seen from Fig. 7 that the first three main vibration modes of the refined model are the lateral vibration mode along the $x$-axis direction, lateral vibration mode along the $y$-axis direction, and torsional vibration modes, which are consistent with the results of the corresponding simplified model in Section 3.3. For the simplified model of the three-layer eccentric structure, the total degree of freedom is nine, and the number of vibration modes is nine. The mass participation coefficients of the vibration mode of the first three modes in the $x$-direction are 72.25, 16.65, and 2.51%, respectively. Their sum is 91.4%, meeting the requirements of exceeding 90%. Therefore, this paper mainly analyzes the vibration characteristics of the first three modes.

**Table 2.** Comparison of the vibration periods of the refined and simplified models

| Mode | Vibration periods [s] | | Relative error [%] | Participation mass coefficient of vibration mode [%] (simplified model) | | |
|---|---|---|---|---|---|---|
| | 3D refined model | Simplified model | | in $x$-direction | in $y$-direction | torsional direction |
| 1 | 0.394 | 0.389 | 1.28 | 72.25 | 8.38 | 10.77 |
| 2 | 0.366 | 0.358 | 2.23 | 16.65 | 61.39 | 13.36 |
| 3 | 0.305 | 0.291 | 4.81 | 2.51 | 21.63 | 67.27 |

## 4. Parametric analysis of translation-torsion coupled vibration characteristics

According to the literature survey (Li and Yin, 1988), $b_y = 0.1 \sim 0.4$, $b_x = 0.2 \sim 0.4$ and $\Omega = 1.0 \sim 1.8$.

### 4.1. Effect of $\Omega$ on the vibration characteristics

Figure 8 displays the variation of the vibration mode direction factors with $\Omega$ in the first stage at $b_x = b_y = 0.2$. With an increased $\Omega$, values of $DX_1$, $DY_2$ and $D\theta_3$ exceed 0.5, while $D\theta_1$, $DX_2$ and $DY_3$ drop below 0.5. At $\Omega < 1.1$, the first mode is the torsional vibration mode, and the second and third vibration modes are lateral vibrations in the two horizontal directions. As $\Omega$ increases, the first three vibration modes change to the lateral vibration mode along the $x$-axis direction, the lateral vibration mode along the $y$-axis direction, and the torsional mode, respectively. This mode transition occurs when $\Omega$ is approximately 1.1. The coupling effect between the torsional and lateral modes becomes weaker with the increase of $\Omega$; therefore, the torsional mode is more challenging to be excited, and the structural response will also be mainly translation. The first-order mode shape is close to the equivalent symmetric system first--order purely lateral vibration mode. Therefore, a larger $\Omega$ value should be taken in the actual design. As $\Omega$ increases from 1.1 to 1.2, $DX_1$ grows by 41.22%; as $\Omega$ further increases from 1.2 to 1.4, $DX_1$ increases by 25.71%. When $\Omega$ exceeds 1.4, the change of $DX_1$ becomes more stable. According to many calculation results, the value of $\Omega$ plays a vital role in the first three orders of the translation-torsion coupled vibration mode at $\Omega = 1 \sim 1.4$. For $b_x \geqslant 0.3$ and $\Omega > 1.6$, the mean variation amplitude of the frequency is only 1.51%, being almost unaffected by $\Omega$. The range of $\Omega$ that plays a key role is within $1 \sim 1.6$. It is suggested that the limiting value of $\Omega$ should be set as different values when designing and analyzing structures with different eccentric degrees.

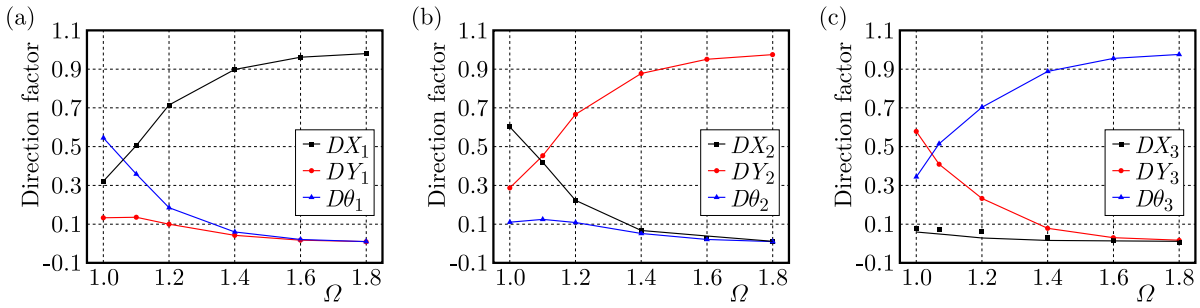


Fig. 8. Variation of the directional factor versus $\Omega$ in the first stage: (a) first mode, (b) second mode, (c) third mode

When the value of $DX_1$ in the second stage approaches 1 (as shown in Fig. 9), $DY_2$ and $D\theta_3$ exceed 0.5, while values of $D\theta_2$ and $DY_3$ are below 0.5. The first-order mode shape approaches the purely lateral vibration mode along the $x$-axis direction, accompanied by a weakened translation-torsion coupled effect. The effect of $\Omega$ on the first-order vibration mode becomes weakened. With an increase of $\Omega$, the second vibration mode changes from torsion to translation in the $y$-direction. And the third-order vibration mode change to the torsional mode. With the increasing external load, the lateral-resisting members along the load direction gradually yield, thereby reducing the total lateral stiffness in this direction. However, full torsional capacity is not weakened much at this stage. Therefore, the first vibration mode of the structure at this stage is mainly lateral motion along the $x$-direction.

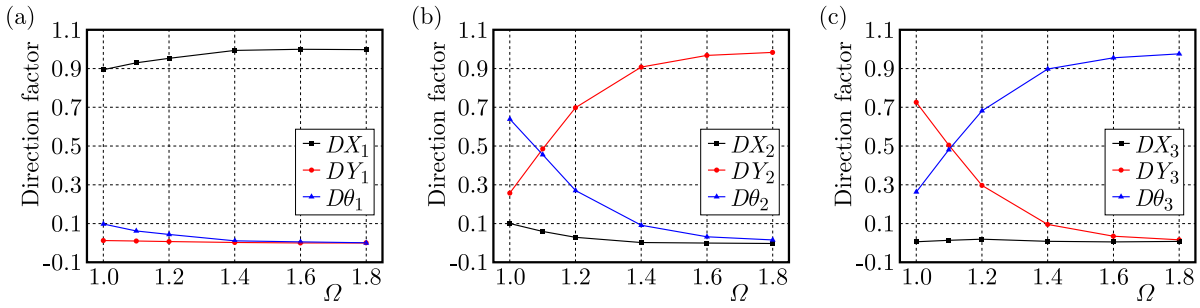


Fig. 9. Variation of the directional factor versus $\Omega$ in the second stage: (a) first mode, (b) second mode, (c) third mode

Figure 10 shows the variation trends in the third stage. As $\Omega$ further increases, $DX_1$ approximately equals 1, $D\theta_2$ and $DY_3$ are less than 0.5, and the corresponding $DY_2$ and $D\theta_3$ exceed 0.5. The value of $\Omega$ corresponding to transformation of the vibration mode is larger than the value in the second stage. At this stage, most of the members along the load direction enter the yield, so the lateral stiffness in this direction decreases significantly. Compared with the second stage, the torsional stiffness of the structure also reduces to varying degrees. The first-order vibration mode is approach to purely lateral mode along the load direction and, simultaneously, the translation-torsion coupled effect becomes weak. When the torsional stiffness is minor, the second and third modes are torsional and lateral modes along the $y$-direction, respectively. At a significant torsional stiffness ($\Omega > 1.2$), the second-and third-order vibration modes turn to the lateral mode along the $y$-axis direction and the torsional vibration mode, respectively. It is worth mentioning that the differences in the directional factors of the primary mode in the second and third modes decrease, and the translation-torsion coupled effects are enhanced.

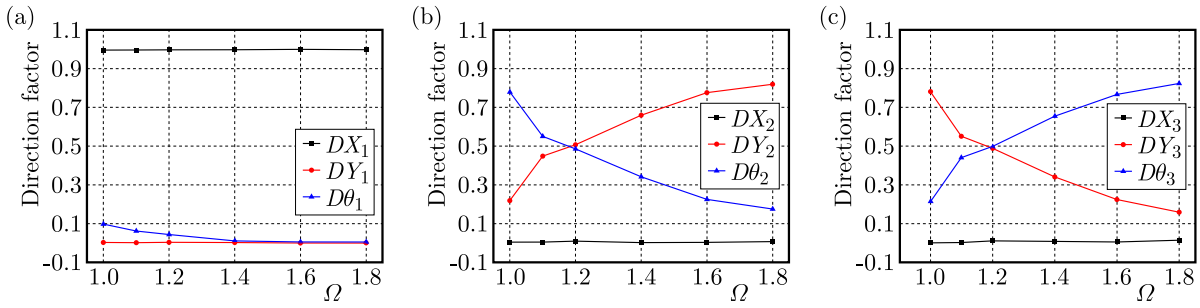


Fig. 10. Variation of the directional factor versus $\Omega$ in the third stage: (a) first mode, (b) second mode, (c) third mode

### 4.2. Effects of $b_x$ and $b_y$ on the vibration characteristics

The variation curves of $DX_i$, $DY_i$ and $D\theta_i$ in the first stage versus $b_x$ and $b_y$ at $\Omega = 1.2$ are evaluated in Fig. 11. It is evident from Fig. 11 that when $b_x = 0.2$, the increase of $b_y$ does not change the primary mode of each mode. At $b_y = 0.1$, $b_x \geqslant 0.3$ or $b_y = 0.2$, $b_x = 0.4$, the first-order vibration mode changes from the lateral mode along the $x$-direction to that along the $y$-axis direction. Further, with an increase in $b_y$ ($b_y \geqslant 0.3$), the first-order vibration mode changes to lateral mode along the $x$-axis direction, and the lateral mode directional factors increase. Through calculation via the model at $\Omega = 1.1$, the mutual interaction between bi-directional eccentricities transforms the first- and second-order vibration modes. After the transformation, the translation-torsion coupled effect between the first two vibration modes is enhanced when the value of $b_x$ becomes larger. It turns out that when $\Omega = 1.1 \sim 1.2$, under the interaction of bi-directional eccentricities, the first- and second-order vibration modes change each other.

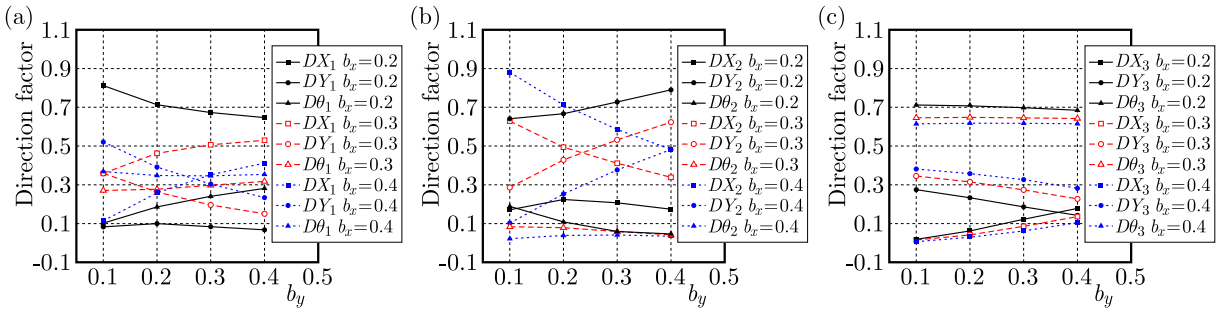


Fig. 11. Variation of the directional factor versus $b_y$ in the first stage: (a) first mode, (b) second mode, (c) third mode

The influences of $b_x$ and $b_y$ on the vibration characteristics in the second stage are given in Fig. 12. It is evident from Fig. 12 that the first three vibration modes are the lateral modes along the $x$- and $y$-directions, and the torsional mode, respectively. Compared with the conditions in the first stage, $DX_1$ increases relatively; the mode directional factors of the second vibration mode change gently with $b_x$ and $b_y$, and $D\theta_3$ changes slightly. The directional mode factors still change with the shift in bi-directional eccentricities. However, this change is insufficient to change the principal vibration directions of each mode. The members in the load direction yield continuously, making the structure lateral stiffness decrease gradually. Hence, lateral motion of the first-order vibration mode increases along the $x$-axis direction. Meanwhile, the torsional stiffness drops slightly, and the torsional factor in the third-order vibration model varies slightly. The effects of bi-directional eccentricities on the vibration mode are gradually weakened.

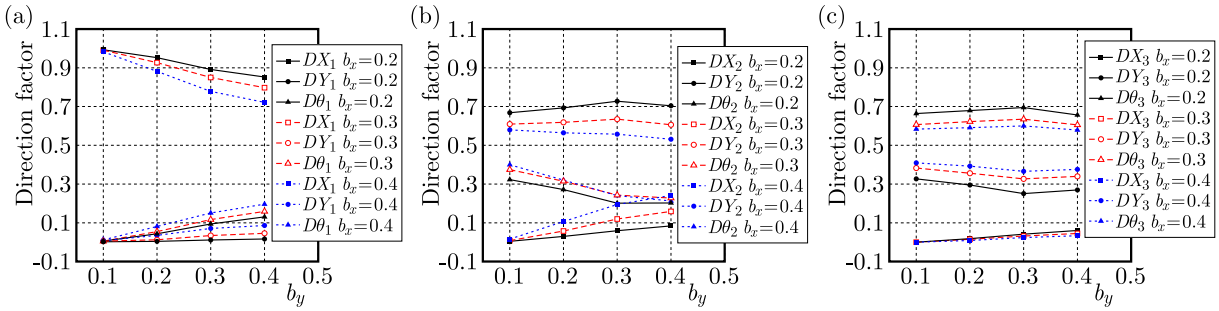


Fig. 12. Variation of the directional factor versus $b_y$ in the second stage: (a) first mode, (b) second mode, (c) third mode

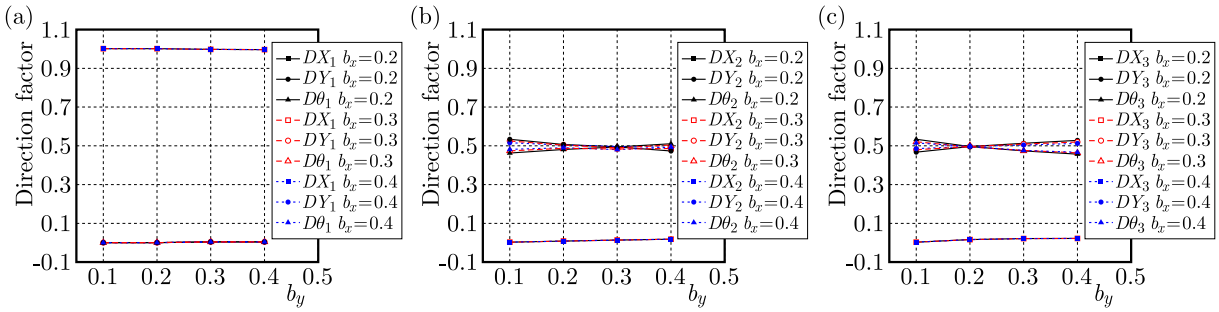


Fig. 13. Variation of the directional factor versus $b_y$ in the third stage: (a) first mode, (b) second mode, (c) third mode

Figure 13 displays the variation trends in the third stage. The change of the mode direction factors with the bi-directional eccentricities is remarkably smooth, suggesting that the development of elastic-plastic further weakens the effect of the bi-directional eccentricities on

the vibration characteristics. The first-order vibration is almost purely lateral mode along the $x$-axis direction. $DY_2$ and $D\theta_3$ are close to 0.5. As $b_x$ and $b_y$ values reach or even exceed 0.3, the second-and third-order vibration modes transform into each other. In the third stage, the lateral stiffness along the $x$-axis direction is weakened significantly, reducing the overall torsional stiffness. However, the members in the non-force direction are still in the elastic stage. Therefore, torsion dominates the second-order vibration mode at large eccentricities. The translation--torsion coupled effect between lateral motion along the $x$-axis and torsion in the first mode is further reduced. However, the translation-torsion coupled effects between the lateral movement along the $y$-axis direction and the torsional ones in the second and third modes are enhanced to a certain degree.

## 5. The proposed approach and discussion

Existing literature studies show that mass eccentricity, stiffness eccentricity, uncoupled torsion to lateral frequency ratios, natural vibration period and strength eccentricity influence the elastic--plastic torsional response in multi-story eccentric structures (Halabian and Birzahandi, 2014; Wu *et al.*, 1999). In particular, the stiffness eccentricity produced due to the center of mass and rigidity is the main reason for the torsional behavior of a building when it is excited by seismic forces. The greater the eccentricity between the center of rigidity and mass, the more prominent the torsional effects (Sneha and Durgaprasad, 2022). The primary purpose of this paper is to reveal the influence of $\Omega$ and bi-directional eccentricities on the dynamic characteristics of the eccentric structure in different elastic-plastic development stages. According to the research in this paper, the stiffness and mass center of the structure should coincide in the structural design, or the stiffness eccentricity should be reduced as much as possible. If the structural plane is irregularly arranged to meet the functional requirements, it is recommended to increase $\Omega$. To make the first-order primary vibration mode translational, and the corresponding mode directional factor not less than 0.9, the recommended limit of $\Omega$ is as follows: when $b_x$ and $b_y$ are less than or equal to 0.2, $\Omega$ should be no less than 1.4. At $0.2 < b_y$ and $b_y < 0.3$, $\Omega$ should be no less than 1.6. In this way, the coupling effect of the first mode will be significantly weakened, and the first mode is close to the first-order purely lateral mode of the equivalent symmetric system. Under the external load, the structural response will be closer to the translational response.

Previous studies have shown that the strength eccentricity significantly influences the displacement and ductility requirements of irregular structures under earthquakes (Sadashiva *et al.* 2012). The yield strength coefficient is used to control the strength distribution between floors in the Code for Seismic Design of Buildings, but there is no provision for the strength distribution of members on the same floor; and the limits of vertical stiffness and strength irregularities are also defined separately (GB50011-2010, 2016). The strength and stiffness of the lateral force resisting members are interdependent, and the strength and stiffness vary together. It is necessary to examine the effects of strength and stiffness distribution combination on the displacement and ductility responses in the seismic response study of asymmetric systems. It is also meaningful to introduce a design guideline for strength/stiffness distributions among lateral force resisting elements for designers to minimize the torsional component in the seismic response. A related research can be taken into consideration for future works.

## 6. Conclusions

The results obtained make it possible to draw the following conclusions:

- It is apparent that the variation curves of the natural vibration frequency of the eccentric frame structures show a general law of three-stage evolution from an elastic to elastic-

-plastic state. The three stages are then simplified. In particular, the variation curve of the natural vibration frequency versus the loading coefficient in the second stage, which plays a vital role in the present analysis, is fitted into a straight line. On this basis, three stages are defined in this study to facilitate parametric analysis of the whole loading process for different elastic-plastic development stages.

- At larger values of $\Omega$, the coupling effect between the torsional and lateral vibration modes is weaker, the torsion mode is more challenging to be excited, and the first-order vibration mode is closer to the first-order purely lateral mode of the equivalent symmetric system. To make the first-order main vibration mode translational and keep the corresponding directional mode factor above 0.9, the recommended limit of $\Omega$ is as follows: if $b_x$ and $b_y$ do not exceed 0.2, $\Omega$ should be no less than 1.4. At $0.2 < b_y < 0.3$, $\Omega$ should be no less than 1.6.
- In the first stage, at $\Omega = 1.1 \sim 1.2$, the coupling effect between bi-directional eccentricities leads to transformation between the first- and second-order vibration modes. At that moment, the direction with the lowest lateral stiffness could not be directly judged as the structure first-order principal vibration direction.
- In the second stage, the enlarging of $b_x$ and $b_y$ do not change the principal vibration modes of various orders. The effects of eccentricities on the translation-torsion coupled vibration characteristics and the translation-torsion coupled effect in the first mode are reduced. In the third stage, as $b_x$ and $b_y$ values reach or even exceed 0.3, the second- and third-order vibration modes transform into each other. The translation-torsion coupled effects between lateral motion along the non-force direction and the torsional ones in the second and third modes are enhanced to a certain degree.

*Acknowledgment*

The research was supported by the High-Level Talents Project of North China University of Water Resources and Electric Power (201803003).

## References

1. Alaa K.M., El-Kashif K.F., Salem H.M., 2022, New definition for torsional irregularity based on floor rotations of reinforced concrete buildings, *Journal of Engineering and Applied Science*, **69**, 1, 1-35
2. Chopra A.K., 2006, *Dynamics of Structures: Theory and Applications to Earthquake Engineering* (in Chinese), translated by Xie L.L., Lv D.G., Beijing, Higher Education Press, 2nd Ed.
3. Duan X.N., Chandler A.M., 1993, Inelastic seismic response of code-designed multistorey frame buildings with regular asymmetry, *Earthquake Engineering and Structural Dynamics*, **22**, 431-445
4. Gao D.Y., 1988, Simplified calculation on cross-section moment and curvature of rectangular cross-section member, *Journal of Zhengzhou University, Engineering Science*, **9**, 1, 9-17
5. GB 50009-2012, 2012, *Load Code for the Design of Building Structures* (in Chinese), Beijing, China Architecture and Building Press
6. GB 50011-2010, 2016, *Code for Seismic Design of Buildings* (2016 Edition) (in Chinese), Beijing, China Architecture and Building Press
7. Georgoussis G.K., Mamou A., 2018, The effect of mass eccentricity on the torsional response of building structures, *Structural Engineering and Mechanics*, **67**, 6, 671-682
8. Halabian A.M., Birzhandi M.S., 2014, Inelastic response of bi-eccentric-plan asymmetric reinforced concrete buildings, *Proceedings of the Institution of Civil Engineers, Structures and Buildings*, **167**, 8, 469-485

9. He Z., Ou J.P., 2007, *Non-Linear Analysis of Reinforced Concrete Structure* (in Chinese), Harbin, Harbin Institute of Technology Press

10. JGJ 3-2010, 2011, *Technical Specification for Concrete Structures of a Tall Building* (in Chinese), Beijing, China Architecture and Building Press

11. Jiang X.L., Kuang Y.P., 2016, Inelastic parametric analysis of two-way asymmetrical multi-storey buildings, *Advances in Structural Engineering*, **19**, 5, 806-824

12. Kewalramani M.A., Syed Z.I., 2020, Seismic analysis of torsional irregularity in multi-storey symmetric and asymmetric buildings, *Eurasian Journal of Analytical Chemistry*, **13**, 3, 286-292

13. Khanal B., Chaulagain H., 2020, Study of seismic response demands of different L-shaped buildings, *Himalayan Journal of Applied Science and Engineering*, **1**, 1, 22-29

14. Kuang Y.P., Jiang X.L., Jiang N., 2018, Inelastic parametric analysis of seismic responses of multistorey bidirectional eccentric structure, *Shock and Vibration*, 1-20

15. Li H.N., Yin Z.Q., 1988, Torsionally coupled response of eccentric structures to multi-dimensional ground motions (in Chinese), *Journal of Earthquake Engineering and Engineering Vibration*, **8**, 4, 45-53

16. Raheem S.A., Ahmed M.M., Ahmed M.M., Abdel-Shafy A.G.A., 2018a, Evaluation of plan configuration irregularity effects on seismic response demands of L-shaped MRF buildings, *Bulletin of Earthquake Engineering*, **16**, 3845-3869

17. Raheem S.A., Ahmed M.M., Ahmed M.M., Abdel-Shafy A.G.A., 2018b, Seismic performance of L-shaped multi-storey buildings with moment-resisting frames, *Proceedings of the Institution of Civil Engineers, Structures and Buildings*, **171**, 5, 395-408

18. Raheem S.A., Omar M., Zaher A.A., Taha A., 2018c, Effects of numerical modeling simplification on seismic design of buildings, *Coupled Systems Mechanics*, **7**, 6, 731-753

19. Rashidi A., Majid T.A., Fadzli M.N., Faisal A., Noor S.M., 2017, A comprehensive study on the influence of strength and stiffness eccentricities to the on-plan rotation of asymmetric structure, *AIP Conference Proceedings*, **1892**, 1, 120013

20. Sadashiva V.K., MacRae G.A., Deam B.L., 2012, Seismic response of structures with coupled vertical stiffness-strength irregularities, *Earthquake Engineering and Structural Dynamics*, **41**, 1, 119-138

21. Sneha K.K., Durgaprasad J., 2022, An investigation of coefficient of torsional irregularity for irregular buildings in plan, *Lecture Notes in Civil Engineering*, **162**, 637-656

22. Stathopoulos K.G., Anagnostopoulos S.A., 2003, Inelastic earthquake response of single-story asymmetric buildings: an assessment of simplified shear-beam models, *Earthquake Engineering and Structural Dynamics*, **32**, 12, 1813-1831

23. Stathopoulos K.G., Anagnostopoulos S.A., 2005, Inelastic torsion of multistorey buildings under earthquake excitations, *Earthquake Engineering and Structural Dynamics*, **34**, 12, 1449-1465

24. Wu R.F., Cai X.H., Qu N.S., 1999, Study on inelastic torsional coupled seismic response of multi-story and high-rise buildings (in Chinese), *Journal of Dalian University of Technology*, **39**, 4, 471-477

25. Yang S.R., Zhang S.Y., 1988, Perturbation solutions of elastic earthquake response of a class of torsionally coupled multi-storey buildings, *Earthquake Engineering and Engineering Vibration*, **8**, 2, 68-78

*Manuscript received April 20, 2022; accepted for print June 7, 2022*